J Mater Sci: Mater Electron (2008) 19:720–726
DOI 10.1007/s10854-007-9390-6

# A graphical peak analysis method for characterizing impurities in SiC, GaN and diamond from temperature-dependent majority-carrier concentration

**Hideharu Matsuura**

Received: 12 May 2007 / Accepted: 21 August 2007 / Published online: 12 September 2007
© Springer Science+Business Media, LLC 2007

**Abstract** A method for uniquely determining the densities and energy levels of impurities from the temperature dependence of the majority-carrier concentration in wide band gap semiconductors (e.g., SiC, GaN, and diamond) is discussed. It is demonstrated that the proposed graphical peak analysis method can evaluate the number of impurity species and can determine those densities and energy levels uniquely and accurately, while fitting a simulation to the experimental temperature-dependent majority-carrier concentration leads to less reliable densities and energy levels of impurities. In the case that the Fermi levels in *p*-type SiC, GaN and diamond are located between the acceptor level and the valence band maximum, the excited states of acceptors strongly affect the hole concentration. This indicates the distribution function including the influence of the excited states should be applied to determine the densities and energy levels of acceptors from the temperature-dependent hole concentration.

## 1 Introduction

Wide band gap semiconductors are regarded as promising semiconductors for devices operating at high temperatures. In order to design optimum device structures, it is necessary to simulate their electric characteristics for a wide range of temperatures from startup temperatures to steady-operation temperatures. Therefore, it is essential to determine the parameters (e.g., densities and energy levels of dopants) required to carry out the device simulations. Moreover, it is important to understand the behavior of impurities in these semiconductors.

Using the temperature-dependent majority-carrier concentration (i.e., $n(T)$ for electrons or $p(T)$ for holes), the density and energy level of one donor species are usually evaluated from the ln $n(T)$–$1/T$ or ln $p(T)$–$1/T$ curve. However, this analysis cannot be applied to semiconductors with more than one type of dopant or a compensated semiconductor. Moreover, it is difficult to obtain reliable values by fitting a simulation to the experimental data, because it is necessary to assume the number of impurity species before the curve-fitting procedure.

Without any assumptions regarding impurity species, free carrier concentration spectroscopy (FCCS) can determine the densities and energy levels of impurities [1]. The FCCS signal is defined as [2, 3]

$$H(T, E_{\mathrm{ref}}) \equiv \frac{n(T)^2}{(kT)^{5/2}} \exp\left(\frac{E_{\mathrm{ref}}}{kT}\right) \tag{1}$$

or

$$H(T, E_{\mathrm{ref}}) \equiv \frac{p(T)^2}{(kT)^{5/2}} \exp\left(\frac{E_{\mathrm{ref}}}{kT}\right), \tag{2}$$

and it has a peak at the temperature corresponding to each impurity level, where $k$ is the Boltzmann constant and $E_{\mathrm{ref}}$ is the parameter that can shift the peak temperature of $H(T, E_{\mathrm{ref}})$ within the measurement temperature range. From each peak, the density and energy level of the corresponding impurity can be accurately determined.

Since the energy levels ($E_{\mathrm{A}}$) of substitutional acceptors in *p*-type SiC, GaN, and diamond are deep, the distribution

H. Matsuura (✉)
Department of Electronic Engineering and Computer Science, Osaka Electro-Communication University, 18-8 Hatsu-cho, Neyagawa, Osaka 572-8530, Japan
e-mail: matsuura@isc.osakac.ac.jp

function including the influence of the excited states of the acceptor $f(E_A)$ is required to analyze their experimental $p(T)$ [3–6], instead of the Fermi-Dirac distribution function $f_{FD}(E_A)$ that does not include this influence.

$$f_{FD}(E_A) = \frac{1}{1 + 4\exp\left(-\frac{E_F(T)-E_A}{kT}\right)} \quad (3)$$

and

$$f(E_A) = \frac{1}{1 + g_A(T)\exp\left(-\frac{E_F(T)-E_A}{kT}\right)}, \quad (4)$$

where $E_F(T)$ is the Fermi level at $T$, $g_A(T)$ is here called the effective acceptor degeneracy factor, given by [4, 6]

$$g_A(T) = 4\left[1 + \sum_{r=2} g_r \exp\left(\frac{E_r - E_A}{kT}\right)\right]\exp\left(-\frac{\overline{E_{ex,A}(T)}}{kT}\right), \quad (5)$$

$\overline{E_{ex,A}(T)}$ is the ensemble average energy of holes at the ground and excited state levels ($E_r$:$r \geq 2$) of the acceptor at $T$, measured from $E_A$, which is given by [4, 6]

$$\overline{E_{ex,A}(T)} = \frac{\sum_{r=2}(E_A - E_r)g_r\exp\left(\frac{E_r-E_A}{kT}\right)}{1 + \sum_{r=2} g_r\exp\left(\frac{E_r-E_A}{kT}\right)}, \quad (6)$$

and $g_r$ is the ($r$–1)th excited state degeneracy factor of the acceptor.

In this paper, the author reports on his investigation of accurate evaluation of impurities from $n(T)$ or $p(T)$ in SiC, GaN, and diamond using FCCS, and also on his discussion of a suitable distribution function for each dopant species.

## 2 Experiment

Although $n$-type 3C–SiC epilayers with thicknesses of 32 and 80 μm were not doped intentionally (i.e., undoped 3C–SiC), those epilayers included N atoms. The details of the sample preparation were reported earlier [7, 8]. About 10-μm-thick $n$-type and $p$-type 4H–SiC epilayers were grown with several N-doping densities and Al-doping densities, respectively, and the details of the sample preparation were written in Refs. [2, 3]. A 400-μm-thick $p$-type 6H–SiC wafer with the Al-doping density ($C_{Al}$) of approximately $4 \times 10^{18}$ cm$^{-3}$ is called a heavily Al-doped 6H–SiC, while a 4.9-μm-thick $p$-type 6H–SiC epilayer with $C_{Al}$ of approximately $6 \times 10^{15}$ cm$^{-3}$ is called a lightly Al-doped 6H–SiC, and both were purchased by Cree Inc. The Mg-doping density ($C_{Mg}$) in a 2-μm-thick $p$-type GaN was approximately $2 \times 10^{19}$ cm$^{-3}$, while the details of the sample preparation were reported in Ref. [9]. A 1.7-μm-thick $p$-type diamond epilayer with the B-doping density ($C_B$) of approximately $2 \times 10^{17}$ cm$^{-3}$ was grown as described in Ref. [5]. In order to obtain $n(T)$ or $p(T)$, Hall-effect measurements were conducted in van der Pauw configuration.

## 3 Results and discussion

### 3.1 Undoped 3C–SiC

Figure 1 shows $n(T)$ and $E_F(T)$ for the 32-μm-thick undoped $n$-type 3C–SiC, denoted by open and solid circles, respectively. The values of $E_F(T)$ was calculated using

$$E_C - E_F(T) = kT\ln\left[\frac{N_C(T)}{n(T)}\right], \quad (7)$$

where $E_C$ is the bottom of the conduction band, $N_C(T)$ is the effective density of states in the conduction band, given by

$$N_C(T) = N_{C0}k^{3/2}T^{3/2}, \quad (8)$$

$$N_{C0} = 2\left(\frac{2\pi m_e^*}{h^2}\right)^{3/2} M_C, \quad (9)$$

$m_e^*$ is the electron effective mass, $M_C$ is the number of equivalent minima in the conduction band, and $h$ is Planck's constant.

Figure 2 depicts the FCCS signal with $E_{ref} = -2.5 \times 10^{-3}$ eV calculated using Eq. 1 with the experimental $n(T)$ shown in Fig. 1. In the figure, one peak and one shoulder appeared.

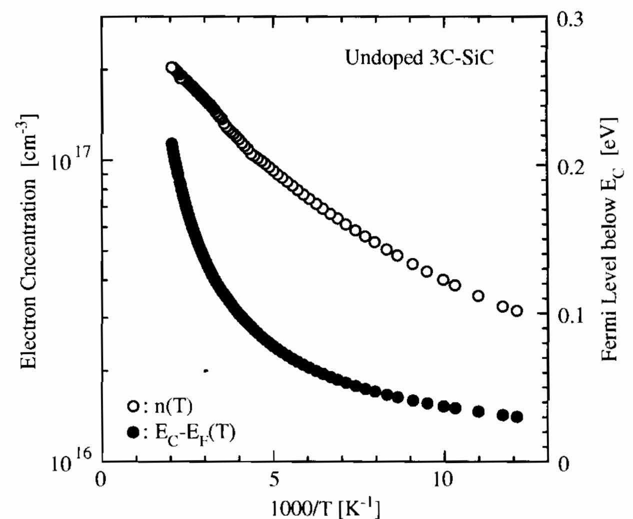


**Fig. 1** Temperature-dependent electron concentration and Fermi level in undoped 3C–SiC

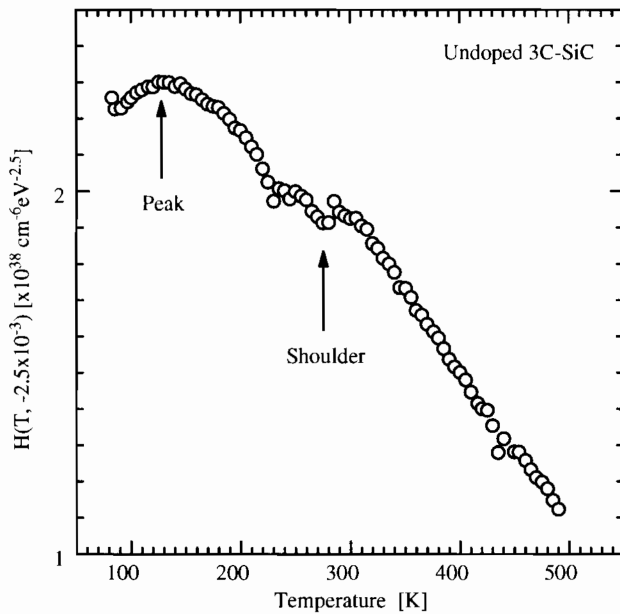


**Fig. 2** FCCS signal with $E_{ref}$ of $-2.5 \times 10^{-3}$ eV for undoped 3C–SiC

Let us consider how to determine the density and energy level of the donor species corresponding to the peak. The FCCS signal is theoretically expressed as [2, 7, 8]

$$H(T, E_{ref}) = \sum_{i=1} \frac{N_{Di}}{kT} \exp\left[-\frac{(E_C - E_{Di}) - E_{ref}}{kT}\right] I(E_{Di}) - \frac{N_{comp} N_{C0}}{kT} \exp\left[\frac{E_{ref} - (E_C - E_F(T))}{kT}\right], \quad (10)$$

where $E_{Di}$ and $N_{Di}$ are the energy level and density of the $i$th donor species, respectively, $N_{comp}$ is the compensating density,

$$I(E_{Di}) = N_{C0} \exp\left(\frac{E_F(T) - E_{Di}}{kT}\right) [1 - f_{FD}(E_{Di})], \quad (11)$$

and $f_{FD}$ $(E_{Di})$ is the Fermi-Dirac distribution function for donors, given by

$$f_{FD}(E_{Di}) = \frac{1}{1 + \frac{1}{2} \exp\left[\frac{E_{Di} - E_F(T)}{kT}\right]}. \quad (12)$$

The function

$$\frac{N_{Di}}{kT} \exp\left[-\frac{(E_C - E_{Di}) - E_{ref}}{kT}\right] \quad (13)$$

in Eq. 10 has a peak value of $N_{Di}$ exp $(-1)/kT_{peaki}$ at a peak temperature of

$$T_{peaki} = \frac{(E_C - E_{Di}) - E_{ref}}{k}. \quad (14)$$

It is clear from Eq. 14 that $E_{ref}$ is the peak-shift parameter. Although $T_{peaki}$ of $H(T, E_{ref})$ is slightly different from $T_{peaki}$ calculated by Eq. 14 due to the temperature dependence of $I(E_{Di})$, we can easily determine the accurate values of $E_{Di}$ and $N_{Di}$ from the peak of the experimental $H(T, E_{ref})$ by a personal computer using the WINDOWS application software for FCCS, which can be freely downloaded at our web site (http://www.osakac.ac.jp/labs/matsuura/).

From the peak temperature of 137 K and the peak value of $2.3 \times 10^{38}$ cm$^{-6}$ eV$^{-2.5}$ in Fig. 2, the energy level ($E_{D2}$) and density ($N_{D2}$) of the corresponding donor species were determined as $E_C - 0.051$ eV, and $7.1 \times 10^{16}$ cm$^{-3}$, respectively.

In order to investigate another donor species included in this epilayer, the FCCS signal of $H2(T, E_{ref})$, in which the influence of the above determined donor species is removed, is calculated using

$$H2(T, E_{ref}) = \frac{n(T)^2}{(kT)^{5/2}} \exp\left(\frac{E_{ref}}{kT}\right) - \frac{N_{D2}}{kT} \times \exp\left[-\frac{(E_C - E_{D2}) - E_{ref}}{kT}\right] I(E_{D2}), \quad (15)$$

as is clear from Eqs. 1 and 10. Figure 3 shows $H2(T, E_{ref})$ with $E_{ref} = -7.0 \times 10^{-3}$ eV. Two peaks appeared. From the lower peak temperature, the energy level ($E_{D1}$), and density ($N_{D1}$) of the corresponding donor species were determined as $E_C - 0.018$ eV, and $3.8 \times 10^{16}$ cm$^{-3}$, respectively, while from the higher peak temperature the energy level ($E_{D3}$), and density ($N_{D3}$) of the corresponding donor species were

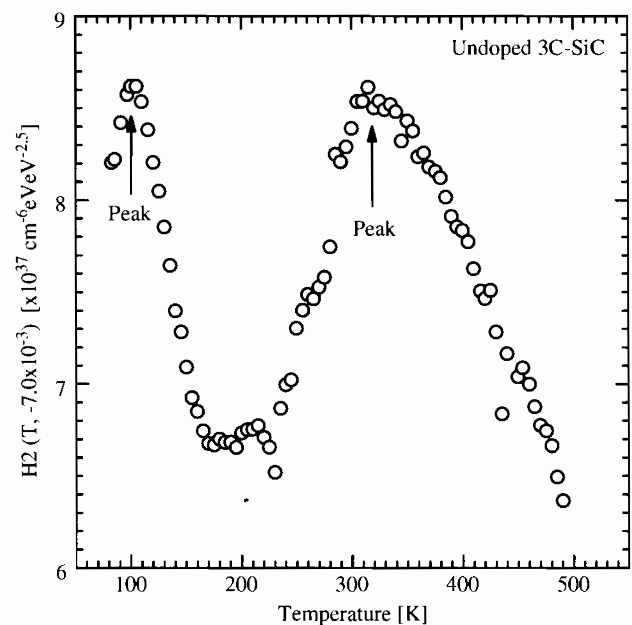


**Fig. 3** FCCS signal with $E_{ref}$ of $-7.5 \times 10^{-3}$ eV for undoped 3C–SiC, in which the influence of the donor species determined in Fig. 2 is removed

determined as $E_C - 0.114$ eV, and $1.1 \times 10^{17}$ cm$^{-3}$, respectively.

In order to verify the values obtained by FCCS, $n(T)$ is simulated using

$$n(T) = \sum_{i=1}^{3} N_{Di}[1 - f_{FD}(E_{Di})] \quad (16)$$

and

$$n(T) = N_C(T) \exp\left(-\frac{E_C - E_F(T)}{kT}\right). \quad (17)$$

The open circles in Fig. 4 represent the experimental $n(T)$, and the solid line represents the $n(T)$ simulation. The solid line is in good agreement with the open circles, indicating that the values determined by FCCS are reliable.

Figure 5 shows the dependence of each donor level on the total donor density ($N_{D,total} = \sum_{i=1}^{3} N_{Di}$), where circles, triangles, and squares represent $E_{D1}$, $E_{D2}$ and $E_{D3}$, respectively. These relationships are expressed as

$$E_C - E_{D1} = 0.054 - 6.3 \times 10^{-8} \sqrt[3]{N_{D,total}} \text{ [eV]}, \quad (18)$$

$$E_C - E_{D2} = 0.078 - 4.2 \times 10^{-8} \sqrt[3]{N_{D,total}} \text{ [eV]}, \quad (19)$$

and

$$E_C - E_{D3} = 0.176 - 9.8 \times 10^{-8} \sqrt[3]{N_{D,total}} hbox[eV], \quad (20)$$

where a unit of $N_{D,total}$ is cm$^{-3}$.

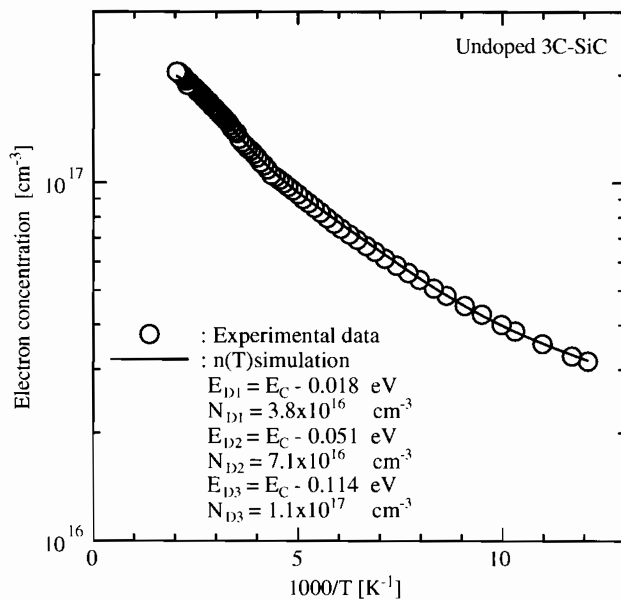


**Fig. 4** $n(T)$ simulation for 3C–SiC

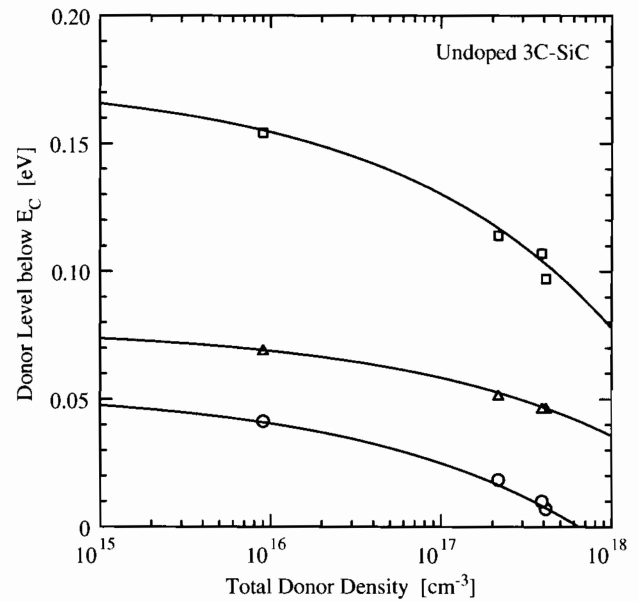


**Fig. 5** Dependence of each donor level on total donor density for undoped 3C–SiC

According to Refs. [7, 8], the donor species with $E_{D2}$ is an isolated substitutional N donor, while the donor species with $E_{D1}$ is considered as some defect-N complex or some nonstoichiometric defect. However, the origin of the donor species with $E_{D3}$ is uncertain up to now.

### 3.2 4H–SiC

In the same way as illustrated for 3C–SiC, the dependence of each donor level on $N_{D,total}$ in N-doped 4H–SiC was investigated. Two types of donor species were detected, and it is found that the relationship between each donor level and $N_{D,total}$ are expressed as

$$E_C - E_{D1} = 0.071 - 3.4 \times 10^{-8} \sqrt[3]{N_{D,total}} \text{ [eV]} \quad (21)$$

and

$$E_C - E_{D2} = 0.124 - 4.7 \times 10^{-8} \sqrt[3]{N_{D,total}} \text{ [eV]}. \quad (22)$$

According to Refs. [10, 11], $E_{D1}$ and $E_{D2}$ correspond to the energy levels of the isolated substitutional N donors at hexagonal and cubic sites in 4H–SiC, respectively.

In the case of Al-doped 4H–SiC, two types of acceptor species were found, and the relationship between the acceptor level ($E_{Ai}$) and the total acceptor density ($N_{A,total}$) are given by

$$E_{A1} - E_V = 0.220 - 1.9 \times 10^{-8} \sqrt[3]{N_{A,total}} \text{ [eV]} \quad (23)$$

and

$$E_{A2} - E_V = 0.413 - 2.1 \times 10^{-7}\sqrt[3]{N_{A,total}}\ \text{[eV]} \quad (N_{A,total} < 1 \times 10^{17}\text{cm}^{-3}) \tag{24}$$

because the acceptor species with $E_{A2}$ could not be detected at $N_{A,total}$ higher than $1 \times 10^{17}$ cm$^{-3}$, where $E_V$ is the top of the valence band. According to Ref. [12], the acceptor species with $E_{A1}$ is an isolated substitutional Al acceptor. Although the origin of the acceptor species with $E_{A2}$ is uncertain up to now, this acceptor species is reported to be related to the Al atom and the carbon vacancy from the study of radiation damage in Al-doped 4H–SiC [13].

### 3.3 Heavily doped *p*-type wide band gap semiconductors

Because in *p*-type wide band gap semiconductors the experimentally obtained $E_A$ (i.e., the ground-state level of acceptors) have been reported to be deep [6], $E_F(T)$ is often between $E_A$ and $E_V$, indicating that the excited states of acceptors are located near $E_F(T)$. Therefore, the excited states must affect $p(T)$.

Figure 6 shows $p(T)$ for the B-doped diamond epilayer, the Mg-doped GaN epilayer, the heavily Al-doped 6H–SiC wafer, and the lightly Al-doped 6H–SiC epilayer, denoted by open diamonds, squares and circles, and solid triangles, respectively.

Figure 7 depicts $E_F(T)$ for the B-doped diamond epilayer, the Mg-doped GaN epilayer, the heavily Al-doped 6H–SiC wafer, and the lightly Al-doped 6H–SiC epilayer, denoted by open diamonds, squares and circles, and solid triangles, respectively. In Fig. 7, moreover, the expected acceptor levels are inserted. The $E_F(T)$ of the B-doped diamond and Mg-doped GaN epilayers and the heavily Al-doped 6H–SiC wafer are located between $E_A$ and $E_V$ in all the measurement temperature range, while the $E_F(T)$ of the lightly Al-doped 6H–SiC is deeper than $E_A$ at almost all measurement temperatures. The $p(T)$ for the diamond and GaN epilayers and the heavily doped 6H–SiC wafer, therefore, must be affected by the excited states of acceptors.

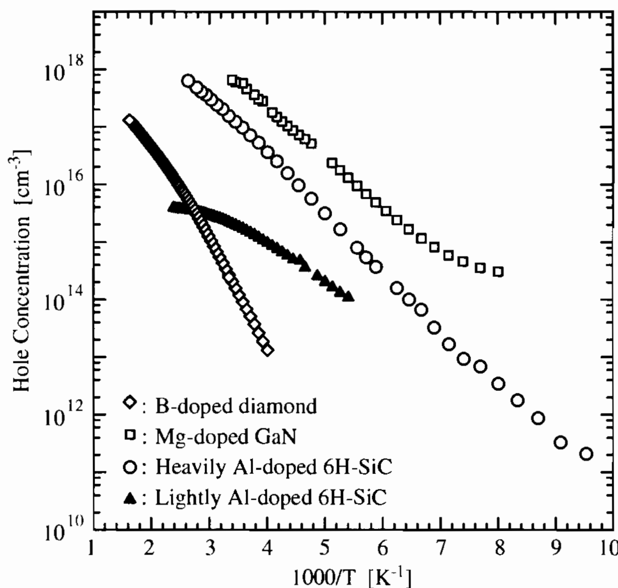


**Fig. 6** Temperature-dependent hole concentrations for B-doped diamond, Mg-doped GaN, and Al-doped 6H-SiC

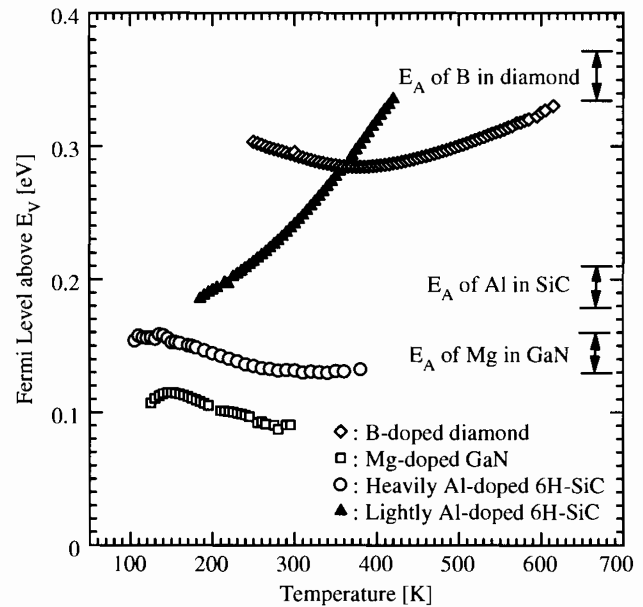


**Fig. 7** Temperature-dependent Fermi levels B-doped diamond, Mg-doped GaN, and Al-doped 6H-SiC

The open circles in Fig. 8 represent the FCCS signal with $E_{ref} = 0.248$ eV, which is calculated using Eq. 2 with the $p(T)$ for the heavily Al-doped 6H-SiC shown in Fig. 6. There was one peak in the figure, and from this peak the acceptor density ($N_A$), $E_A$, and $N_{comp}$ were determined as $2.5 \times 10^{19}$ cm$^{-3}$, $E_V + 0.18$ eV, and $7.3 \times 10^{17}$ cm$^{-3}$ using $f_{FD}(E_A)$, respectively, while those were determined as $3.2 \times 10^{18}$ cm$^{-3}$, $E_V + 0.18$ eV, and $9.0 \times 10^{16}$ cm$^{-3}$ using $f(E_A)$, respectively. The FCCS signal can be simulated with the determined values ($N_A$, $E_A$, and $N_{comp}$) and the experimental $E_F(T)$ shown in Fig. 6 using

$$H(T, E_{ref}) = \frac{N_A}{kT}\exp\left(-\frac{(E_A - E_V) - E_{ref}}{kT}\right) I(E_A) - \frac{N_{comp}N_{V0}}{kT}\exp\left(\frac{E_{ref} - (E_F(T) - E_V)}{kT}\right) \tag{25}$$

and

$$I(E_A) = N_{V0}\exp\left(\frac{E_A - E_F(T)}{kT}\right)F(E_A), \tag{26}$$

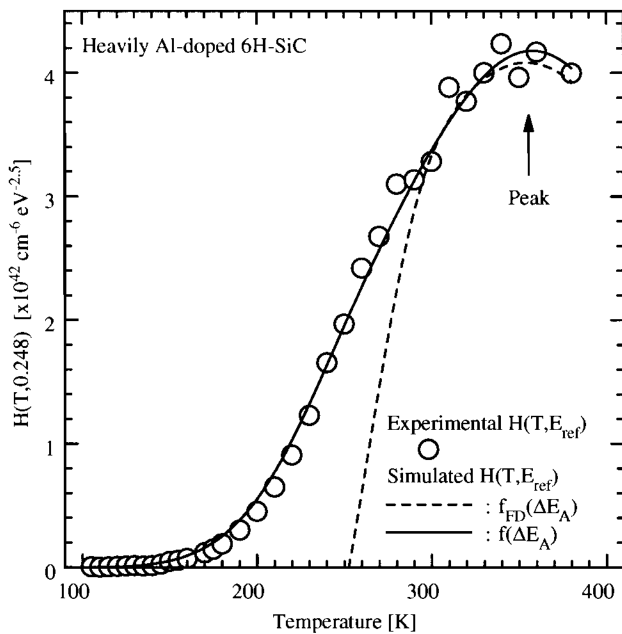


**Fig. 8** FCCS signal with $E_{ref}$ of 0.248 eV for heavily Al-doped 6H-SiC

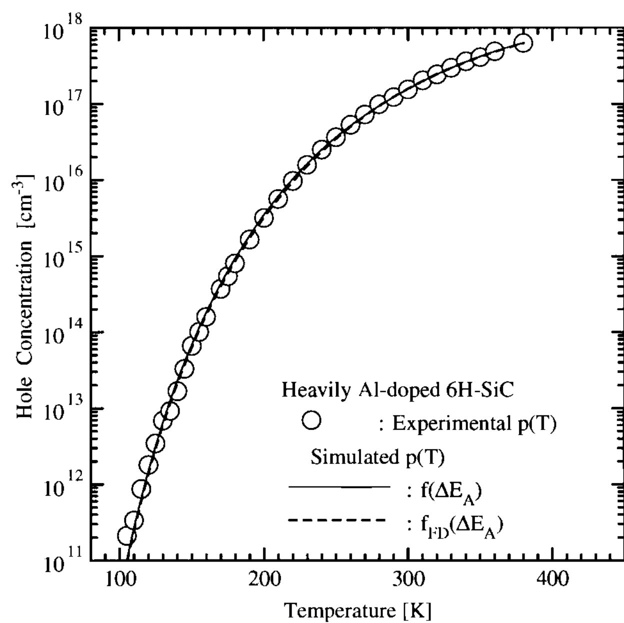


**Fig. 9** $p(T)$ simulation for heavily Al-doped 6H-SiC. The broken line overlaps the solid line

where $N_{V0} = 2(2\pi\, m_h^* /h^2)^{3/2}$, $m_h^*$ is the hole effective mass, and $F(E_A)$ is the distribution function for acceptors, that is, $f_{FD}$ $(E_A)$ or $f(E_A)$. The FCCS simulations for $f_{FD}$ $(E_A)$ and $f(E_A)$ are shown by the broken and solid lines, respectively. As is clear from the figure, the FCCS simulation for $f(E_A)$ is in agreement with the experimental FCCS better than $f_{FD}$ $(E_A)$.

In the same way as illustrated for $n$-type 3C–SiC, the $p(T)$ simulations for $f_{FD}$ $(E_A)$ and $f(E_A)$ were obtained, and are shown by the broken and solid lines in Fig. 9, respectively. In the figure, the broken line overlaps with the solid line. Both the lines are in good agreement with the experimental $p(T)$ shown by circles, though $N_A$ for $f_{FD}$ $(E_A)$ is much higher than $N_A$ for $f(E_A)$. This indicates that it is difficult to determine $N_A$, $E_A$, and $N_{comp}$ by fitting a $p(T)$ simulation to the experimental $p(T)$.

Since the $C_{Al}$ in the heavily Al-doped 6H–SiC was approximately $4 \times 10^{18}$ cm$^{-3}$, the density (i.e., $N_A$) of Al atoms located at substitutional sites should be equal or less than the $C_{Al}$. Therefore, $f(E_A)$ is significantly more appropriate for the distribution function in the heavily doped 6H–SiC than $f_{FD}$ $(E_A)$.

In the lightly Al-doped 6H–SiC, on the other hand, the values of $N_A$, $E_A$, and $N_{comp}$ determined using $f_{FD}$ $(E_A)$ from the peak of the FCCS signal were similar to those using $f(E_A)$. This indicates that both $f_{FD}$ $(E_A)$ and $f(E_A)$ can lead to reliable $N_A$, $E_A$, and $N_{comp}$ when $E_F$ $(T)$ is deeper than $E_A$.

In the same way as illustrated for the heavily Al-doped 6H–SiC, the values of $N_A$, $E_A$, and $N_{comp}$ in the B-doped diamond and Mg-doped GaN epilayers were determined. Those for the B-doped diamond epilayer were evaluated as $9.7 \times 10^{17}$ cm$^{-3}$, $E_V$ + 0.34 eV, and $4.0 \times 10^{16}$ cm$^{-3}$ using $f_{FD}$ $(E_A)$, respectively, while those were determined as $2.8 \times 10^{17}$ cm$^{-3}$, $E_V$ + 0.32 eV, and $2.0 \times 10^{16}$ cm$^{-3}$ using $f(E_A)$, respectively, where the $C_B$ in the epilayer was approximately $2 \times 10^{17}$ cm$^{-3}$. In the Mg-doped GaN epilayer, those were determined as $8.5 \times 10^{19}$ cm$^{-3}$, $E_V$ + 0.15 eV, and $2.3 \times 10^{18}$ cm$^{-3}$ using $f_{FD}$ $(E_A)$, respectively, while those were determined as $6.0 \times 10^{18}$ cm$^{-3}$, $E_V$ + 0.16 eV, and $1.3 \times 10^{17}$ cm$^{-3}$ using $f(E_A)$, respectively, where the $C_{Mg}$ in the epilayer was approximately $2 \times 10^{19}$ cm$^{-3}$. Judging from the difference between $N_A$ and $C_B$ or $C_{Mg}$, it is found that $f(E_A)$ is applicable to substitutional acceptors with deep energy levels for any acceptor density, while $f_{FD}$ $(E_A)$ is limited to the case of $E_F(T)$ deeper than $E_A$.

## 4 Conclusions

Impurities in undoped 3C–SiC epilayers were investigated using the graphical peak analysis method called FCCS. Without any assumptions regarding donor species, three types of donor species were detected, and those densities and energy levels were determined uniquely from $n(T)$. The dependence of each donor level on the total donor density was obtained in $n$-type 3C–SiC and 4H–SiC. Moreover, the relationship between each acceptor level and the total acceptor density in $p$-type 4H–SiC was determined.

In $p$-type 6H–SiC, GaN, and diamond whose $E_F$ ($T$) were located between $E_A$ and $E_V$, it was found that $p(T)$ was strongly affected by the excited states of the acceptor. It was also demonstrated that from experimental $p(T)$ the distribution function $f(E_A)$ including the influence of the excited states led to reliable $N_A$ and $E_A$, not the Fermi-Dirac distribution function $f_{FD}$ ($E_A$) that does not consider the affect of the excited states.

**Acknowledgments** This work was partially supported by the Academic Frontier Promotion Projects of the Ministry of Education, Culture, Sports, Science and Technology in 1998–2002 and 2003–2007, and partially supported by the Grant-in-Aid for Scientific Research of Japan Society for the Promotion of Science in 2006 and 2007.

## References

1. H. Matsuura, K. Sonoi, Jpn. J. Appl. Phys. **35**, L555 (1996)
2. S. Kagamihara, H. Matsuura, T. Hatakeyama, T. Watanabe, M. Kushibe, T. Shinohe, K. Arai, J. Appl. Phys. **96**, 5601 (2004)
3. H. Matsuura, M. Komeda, S. Kagamihara, H. Iwata, R. Ishihara, T. Hatakeyama, T. Watanabe, K. Kojima, T. Shinohe, K. Arai, J. Appl. Phys. **96**, 2708 (2004)
4. H. Matsuura, J. Appl. Phys. **95**, 4213 (2004)
5. H. Matsuura, T. Morizono, Y. Inoue, S. Kagamihara, A. Namba, T. Imai, T. Takebe, Jpn. J. Appl. Phys. **45**, 6376 (2006)
6. H. Matsuura, Phys. Rev. B **74**, 245216 (2006)
7. H. Matsuura, Masuda, Y. Chen, S. Nishino, Jpn. J. Appl. Phys. **39**, 5069 (2000)
8. H. Matsuura, H. Nagasawa, K. Yagi, T. Kawahara, J. Appl. Phys. **96**, 7346 (2004)
9. H. Matsuura, D. Katsuya, T. Ishida, S. Kagamihara, K. Aso, H. Iwata, T. Aki, S.-W. Kim, T. Shibata, T. Suzuki, Phys. Status Solidi C **0**, 2214 (2003)
10. M. Ikeda, H. Matsunami, T. Tanaka, Phys. Rev. B **22**, 2842 (1980)
11. W. Götz, A. Schöner, G. Pensl, W. Suttrop, W.J. Choyke, R. Stein, S. Leibenzeder, J. Appl. Phys. **73**, 3332 (1993)
12. T. Troffer, M. Schadt, T. Frank, H. Itoh, G. Pensl, J. Heindl, H.P. Strunk, M. Maier, Phys. Status Solidi A **162**, 277 (1997)
13. H. Matsuura, S. Kagamihara, Y. Itoh, T. Ohshima, H. Itoh, Physica B **376–377**, 34 (2006)